Deformation-induced phase changes of Zn-Al alloy during ultra-precision raster milling

S.J. Zhang[1, 2], S. To[2, *]

[1]Research Institute of Mechanical Manufacturing Engineering, School of Mechatronics Engineering, Nanchang University, Nanchang, PR China.

[2]State Key Laboratory in Ultra-precision Machining Technology, Department of Industrial and Systems Engineering, The Hong Kong Polytechnic University, Hong Kong, PR China.

* E-mail: Sandy.To@polyu.edu.hk, Tel: +852-2766-6587, Fax: +852-2764-7657

Abstract Metal cutting is a complex material removal process with elastic deformation (ED) and plastic deformation (PD) together taking place in chip formation and surface generation. PD consists of shear PD (SPD) and normal PD (NPD) intrinsically relevant to cutting mechanism, such as pure cutting and ploughing. In ultra-precision machining, PD induces phase changes of Zn-Al alloy once, i.e. phase decomposition. In this study, the distinctive effects of SPD and NPD in surface generation on phase changes of Zn-Al alloy in ultra-precision raster milling (UPRM) with horizontal cutting under up-cutting mode were firstly discussed. At the machined surfaces of Zn-Al alloy, NPD and SPD both results in phase changes, but only NPD changes preferred crystal orientation; and PD under high speed cutting induces phase changes twice, i.e. four-phase transformation occurs after phase decomposition, namely twin phase changes, which were firstly observed.

Keywords Phase change; Normal plastic deformation; Shear plastic deformation; Zn-Al alloy; Ultra-precision raster milling

1. Introduction

In practical cutting, material removal is a complex mechanical maufacturing process. At the being-machined surface, it involves pure cutting (shearing) and ploughing (compressing) [1], named cutting mechanism, accompanying elastic deformation (ED) and plastic deformation (PD) [2, 3] not only in chip formation and but also in surface formation [3, 4]. Essentially, ED and PD together affect components' surface integrity [5, 6], such as surface quality (surface roughness and form error) and surface material properties. Further, surface integrity determines components' quality, life, and stability [6, 7]. Therefore, much attention has been attracted to studying the complex cutting process.

In a general material removal process, more or less ploughing always takes place with pure cutting. Ploughing force is caused majorly by ED and PD of the machined material around tool cutting edge and influenced by tool cutting edge radius [4]. Large cutting edge radius will create more ploughing instead of chip formation [8]. The relationship between ploughing force and tool cutting edge radius has been theoretically and experimentally investigated fully [4, 9-11]. Moreover, the effects of the tool cutting edge radius changed by edge wear on ploughing force have been discussed with details [12, 13]. For ploughing force components, thrust force is more sensitive to tool cutting edge radius or/and edge wear than cutting force, and the cutting force acting on the tool rake face is almost not changed [4, 12, 14]. Additionally, PD covers shear PD (SPD) and normal PD (NPD), which are induced by cutting force and thrust force as orthogonal components of ploughing force, shear force, and friction force, as schematically shown in Figure 1. At the being-machined surface, SPD is corresponding to shear force, friction force component, and ploughing force component in the horizontal direction, i.e. cutting force. In addition, NPD is caused by the friction force component and ploughing force component in the vertical direction, i.e. thrust force. The external stresses are not only left at a deformed chip and but also left at a machined surface layer [3, 4]. Much research has focused on chip formation under PD [15, 16]. However, the different effects of NPD and SPD on surface formation have not been discussed.

In our previous studies [17, 18], phase changes of Zn-Al alloy are an indicator of PD and the phase changes occur in low speed cutting (low strain rate). However, strain rate plays a crucial role in influencing phase transition [19, 20]. Inspired by their work, the phase changes of Zn-Al alloy under high speed cutting (high strain rate) in ultra-precision raster milling (UPRM) were discussed. The distinctive effects of SPD and NPD on phase changes were studied. A tool before and after worn was employed to cut the alloy, which can makes the SPD and NPD contributions to chip deformation and surface formation different at the milled surfaces of Zn-Al alloy. A series of experiments have been conducted through measuring phase changes, chip deformation, crystal orientation, and tool wear features. The SPD and NPD were analyzed with theoretical modeling.

2. Experimental setups

Two prepared eutectoid Zn-Al alloy (76wt%Zn–22wt%Al–2wt%Cu) specimens were treated at 350^{o}C for 4 days and then furnace cooled (FC) to room temperature. Two flat-cutting tests were performed on an UPRM machine with a commercial natural single crystal diamond tool, as shown in Figure 2. It is a five-axis ultra-precision freeform machine system, possessing three linear axes (X, Y and Z) and two rotational axes (B and C). A diamond tool is set up with the spindle and a workpiece is installed on the B axis rotation table.

In the flat-cutting tests, the selected cutting strategy is horizontal cutting, i.e. feed direction is horizontal, and the cutting mode is up-cutting, as shown in Figure 2. The cutting conditions are listed in Table 1, and the tool geometry parameters are presented in Table 2. The cutting speed is very high at 1,360 m/min (2π × 8,000 rpm × 27 mm), which means high strain rate. The new tool was extremely sharp with a tool cutting edge radius of 10~20 nm. The coolant was used in order to eliminate heat effect on phase changes of the machined material. It is Clairsol 330 mainly comprised of petroleum distillates (hydrotreated light, kerosene-unspecified).

In practical material removal, SPD and NPD together take place in chip formation and surface formation. In this study, the SPD and NPD at the machined surfaces of Zn-Al alloy were discussed. Due to the extremely sharp tool cutting edge resulting in extremely low thrust force, the SPD is dominant with a little NPD, as schematically shown in Figure 1 (a). When the tool becomes blunt, edge wear results in a substantial increase in thrust force [12], i.e. the NPD substantially increases, as schematically shown in Figure 1 (b). Overall, as edge wear increases tool cutting edge radius to result in a cutting-to-ploughing evolution, the NPD will sensitively increases and the SPD slightly increases. For this reason, the experiment includes three steps.

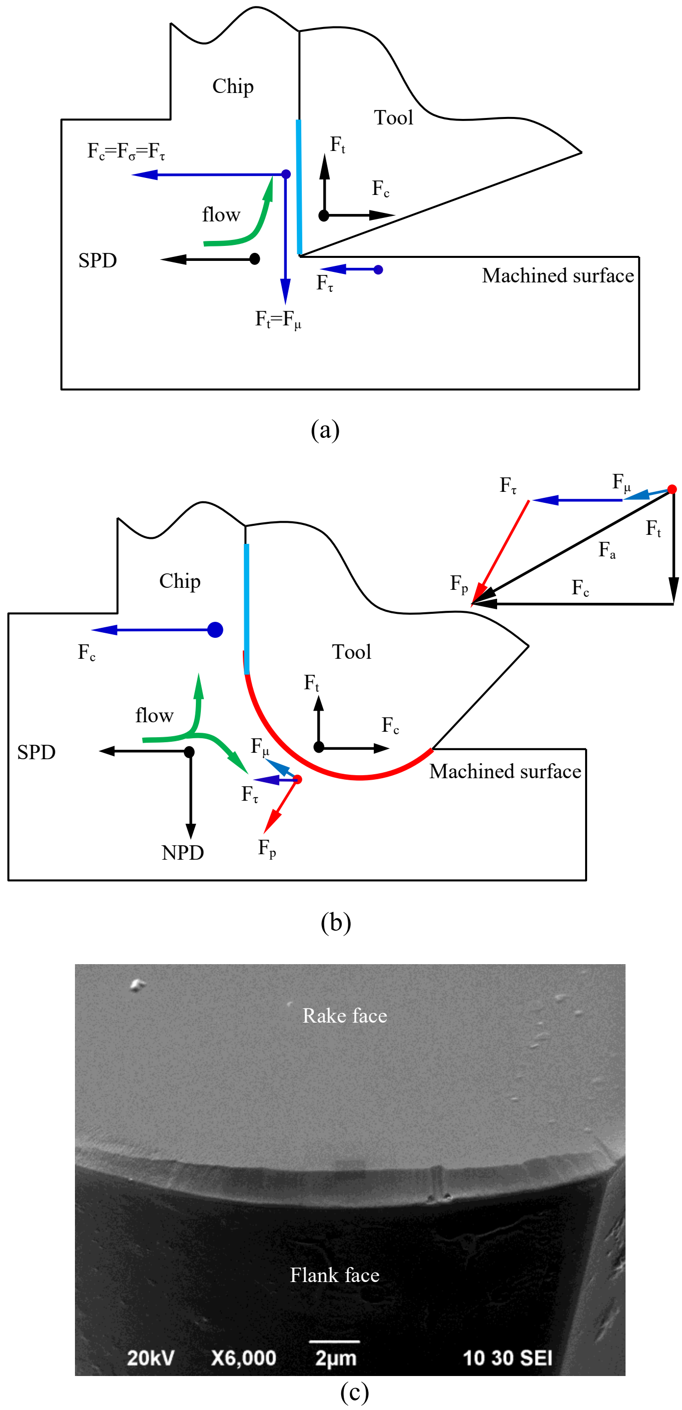

Figure 1. Idealized surface formation with chip formation in: (a) pure cutting and (b) ploughing with force components, and (c) tool wear features (F_t: thrust force; F_c: cutting force; F_τ: shear force; F_p: ploughing force; F_μ: friction force; F_σ: compressive force)

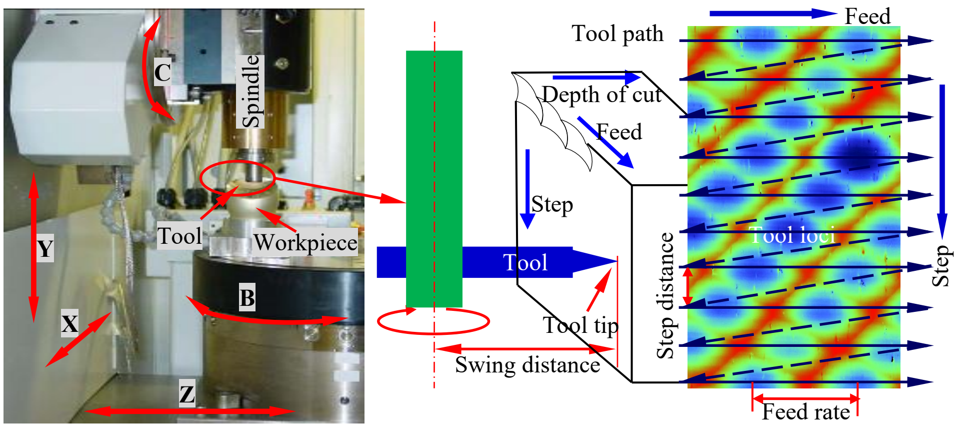

Figure 2. Ultra-precision raster milling with horizontal cutting under up-cutting

Table 1. Cutting conditions

Spindle speed (rpm)	8000
Feed rate (μm/rev.)	5
Depth of cut (μm)	2
Swing distance (mm)	27
Cutting speed (m/min)	1,360
Step distance (μm)	10
Cutting strategy	Horizontal cutting
Cutting mode	Up-cutting
Coolant	On

Table 2. Diamond tool geometry parameters

Tool cutting edge radius (nm)	10~20
Tool rake angle (°)	0
Tool nose radius (μm)	17
Tool clearance angle (°)	15

Firstly, one Zn-Al alloy specimen denoted by Sample 1 was milled by the new tool. Since the tool was too sharp, the SPD dominantly took place with a little NPD at the machined surface. Secondly, the new tool was used to flat-cut copper alloy to produce edge wear, as shown in Figure 1 (c), obtained by scanning electron microscopy (SEM). The worn tool edge radius is up to several micrometers further larger than its original edge radius of 10~20 nm. Finally, the worn tool was employed to mill the other Zn-Al alloy specimen denoted by Sample 2, where more ploughing occurred. Hence, at the machined surface the NPD greatly increased. In addition, the produced chips were simultaneously collected. Each sample was cut at five times with the same cutting conditions. After each cutting tests, the diamond tool was cleansed by high-pressure air with alcohol and observed by optical microscopy (Olympus BX60).

The two specimens after each UPRM were examined immediately. Back-scan electron microscopy (BSEM) and X-ray diffraction (XRD) techniques were employed to detect phase changes. The phases involved in this study are presented in Table 3. The XRD incident angle at 3° was selected in order efficiently to trace phase changes at the deformed surface layers. Hardness and elastic modulus tests of the machined surfaces were performed on a Nano-indenter II (Nano Instruments Inc., Model IIs). A Berkovich nano-indenter (a three-sided pyramidal diamond tip) with a tip radius of 200 nm was employed. It has a high accuracy for the loading as low as 500 μN and for the resolution of the penetration depth to be 0.04 nm. In testing, the hardness and elastic modulus are automatically measured against different loads coordinating with different nano-indentation displacements. Then, the nano-indentation displacements are collected together with the related loads. For each sample, 13 indentations were made at different points with different loads from 0.07 to 300 mN, which was repeated at ten times to calculate the average values of hardness and elastic modulus. The data between the hardness and elastic modulus to the nano-indentation displacement were obtained statistically based on the multi-measured method. Optical microscopy (Olympus BX60) was utilized to observe chip formation.

Table 3 Phases involved in this study (fcc: face-centered cubic; hcp: hexagonal close-packed)

Phase	Description
α	Al rich fcc phase
ε	$CuZn_4$ hcp phase
η	Zn rich hcp phase
T	Distorted $Zn_{10}Al_{35}Cu_{55}$ bcc structure in mass %
$η_T$	Metastable Zn rich hcp phase
$η_{FC}$	Supersaturated Zn rich hcp phase in furnace cooled Zn-Al ally

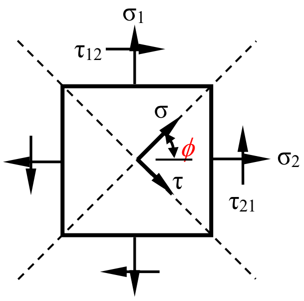

Figure 3. Compressive and shear stresses in a stress infinitesimal element

3. Results and discussion

3.1 Theoretical modeling

In a loaded material body, the stress at each point can be characterized by a stress infinitesimal element. For simplicity, a 2D element is employed in this study, as shown in Figure 3. In addition, some assumptions have to be made: (i) the system is static equilibrium; (ii) only the dominant factors, such as cutting forces, are considered and others are neglected. Therefore, the relationship between compressive stress and shear stress for each infinitesimal element at a machined surface is written as Equation 1, where σ_2=0. Under pure cutting, only SPD occurs where σ_1=0, i.e. Equation 1 is rewritten as Equation 2. Under the cutting-ploughing mode, SPD and NPD together occur, i.e. Equation 1 is rewritten as Equation 3. As comparing Equation 2 with Equation 3, the difference is the NPD, i.e. σ_1. Generally, due to edge wear resulting in a cutting-to-ploughing evolution, the NPD substantially increases and the SPD slightly increases. Accordingly, it is ideally assumed that the SPD is only determined by material yield limit (material damage criterion [21]) when cutting. Therefore, the SPD is considered constant. The equations well explain the model in Figure 3.

$$\begin{cases} \sigma = \dfrac{\sigma_1+\sigma_2}{2} + \dfrac{\sigma_1-\sigma_2}{2}\cos 2\phi + \tau_{12}\sin 2\phi \\ \tau = -\dfrac{\sigma_1-\sigma_2}{2}\sin 2\phi + \tau_{12}\cos 2\phi \end{cases} \tag{1}$$

$$\begin{cases} \sigma = \tau_{12}\sin 2\phi \\ \tau = \tau_{12}\cos 2\phi \end{cases} \tag{2}$$

$$\begin{cases} \sigma = \dfrac{\sigma_1}{2}(1+\cos 2\phi) + \tau_{12}\sin 2\phi \\ \tau = -\dfrac{\sigma_1}{2}\sin 2\phi + \tau_{12}\cos 2\phi \end{cases} \tag{3}$$

3.2 Phase changes

Figure 4 shows the BSEM and XRD results of Zn-Al alloy before and after being milling with a new tool and the worn tool, respectively. Figure 4(a1), (b1) and (c1) shows the BSEM results of the raw sample, Sample 1 and Sample 2, respectively. It is clearly observed that the α phase precipitated in the light-imaged η_T phase. It has been reported in Refs. [18, 22] that $\eta_{FC}\rightarrow\eta_T+\alpha+\varepsilon$. Surprisingly, the α phase of Sample 2 is not more than that of Sample 1, which is contrary to that the more PD induces the more α phase precipitation [18].

The XRD results are shown in Figure 4 (a2) for the raw Zn-Al alloy specimen before milled and Figure 4 (b2) and (c2) for Sample 1 and Sample 2, respectively. The evolvement of (0002) η_T means the η_{FC} phase decomposition induced by an external stress during UPRM and its intensity also decreased. The same result has been reported by To et al. [5, 17, 18]. Reversely, the relative intensity of (0002) η_T of Sample 2 is further higher than that of Sample 1, which all are higher than that of the raw sample before milled. In addition, the relative intensities of the phases ε and α are almost the same, which matches well the BSEM results in Figure 4 (b1) and (c1), but more than that of the raw sample before milled, as shown in Figure 4 (a1) and Figure 4(a2). The peak amplitude indicates partial stress relieving.

From the BSEM and XRD results, the relative intensities of the phases ε and α are the same for the milled samples with the tool before and after worn, but the relative intensity of the phase (0002) η_T increases. The only reason is that four-phase transformation simultaneously occurred, i.e. $\alpha+\varepsilon\rightarrow T+\eta$, known as quenching, when the η_{FC} phase decomposed, namely twin phase changes. As compared with the previous results [17, 18], the difference is that the cutting speed is high, i.e. high strain rate. Therefore, it can be inferred that under high speed cutting (high strain rate) phase decomposition and four-phase transformation together take place and edge wear promotes phase decomposition and four-phase transformation through SPD and NPD.

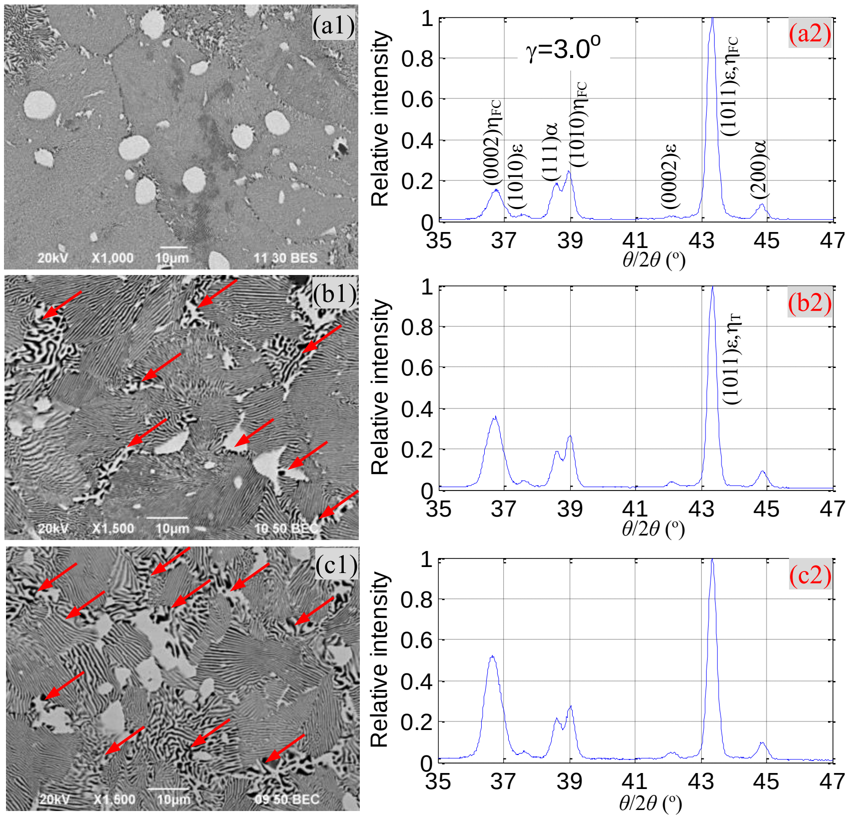

Figure 4. Phase changes indicated by (1) BSEM images and (2) XRD patterns of Zn-Al alloy (a) before milled, and after milled: (b) Sample 1 and (c) Sample 2 (←: α phase precipitation)

3.3 Nano-indentation testing and chip deformation

Nano-hardness tests were conducted to measure surface hardness and modulus of Sample 1 and Sample 2. In Figure 5 (a1) and (a2), the corresponding hardness to penetration depth is plotted for the two samples. A very thin hardened layer was generated at the two raster-milled surfaces. Sample 2 possesses a thicker deformation layer at about 500 nm and Sample 1 has a thinner one at about 100 nm. It means that the edge wear strongly degenerated the surface layer. According to the proposed-above XRD and BSEM results, the heavier phase changes took place at the more greatly deformed surface layer with the worn tool; and the thinner deformed surface layer was formed with the slighter phase changes with the new tool.

The corresponding elastic modulus of the raster-milled surfaces for the two samples is plotted in Figure 5 (b1) and (b2). Figure 5 (b1) shows that the corresponding modulus of Sample 1 slightly increases and then gradually decreases. However, in Figure 5 (b2), the modulus of Sample 2 only decreases, and the surprising transition took place. It indicates that as ploughing had a significant impact on surface deformation in the cutting process, since edge wear enhanced NPD at the machined surface, where more four-phase transformation after phase decomposition occurred. Therefore, edge wear resulted in the transition with great phase changes through substantial NPD.

In a material removal process, chip deformation is an indirect indicator of SPD and NPD in surface formation. The corresponding chips were imaged by an optical microscopy, as shown in Figure 5 (c1) and (c2). The sheet-chips were produced when milling Sample 1 as shown in Figure 5 (c1) and the catastrophic stripes were formed for Sample 2 as shown in Figure 5 (c2). It indicates that the chips were generated neatly with the new tool but the chips were produced laboriously with the worn tool. Accordingly, it reflects that the more NPD took place at the machined surface with the worn tool than that with the new tool, which reasonably supports the above results.

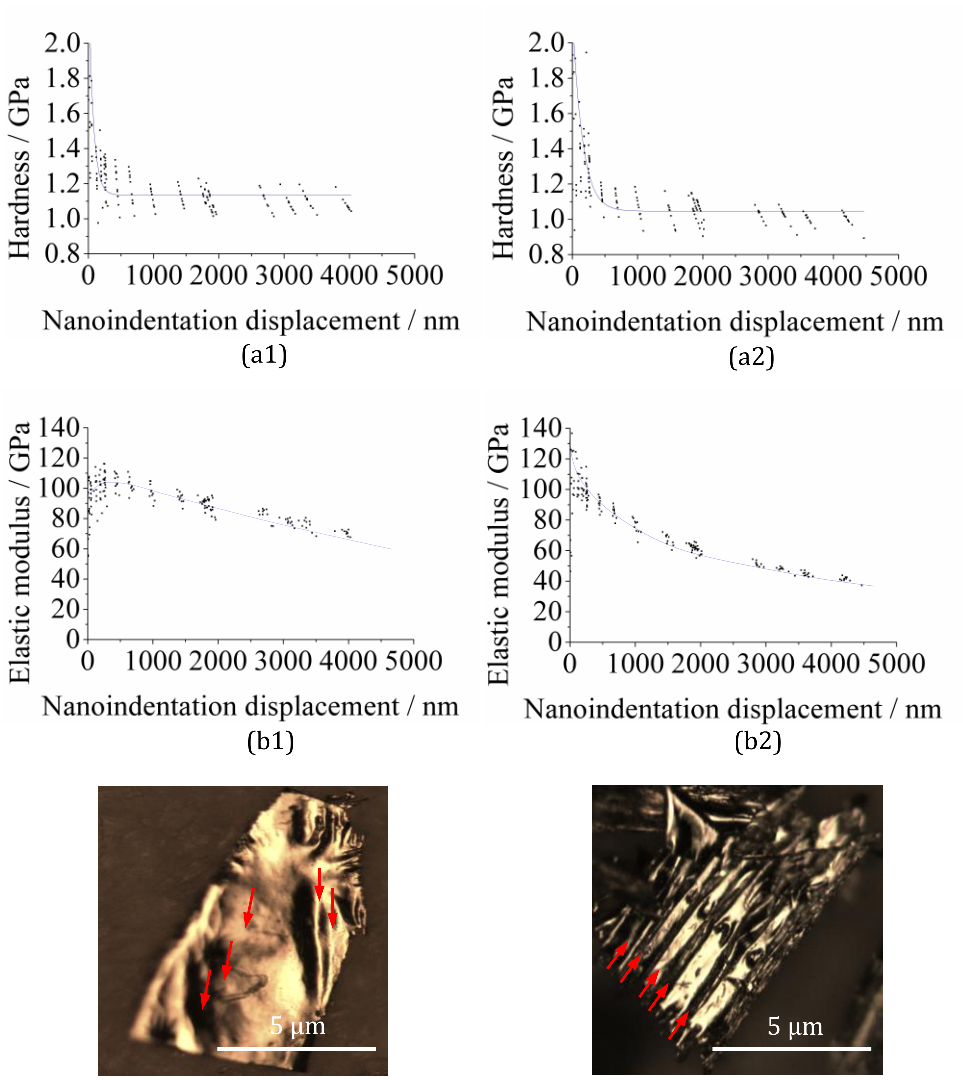

Figure 5. Nano-indentation testing of Zn-Al alloy: (a) surface hardness, (b) surface elastic modulus and (c) chips of (1) Sample 1 and (2) Sample 2

3.4 Crystal orientation changes

Accompanying UPRM-induced phase changes, preferred crystal orientation was evolved at the raster-milled surface layers [18]. The peak shift indicates residual stress. From the XRD results, as shown in Figure 4, the Braggle angle for the (0002) η / $\eta_{T/FC}$ phase was obtained. The Braggle angle for the raw FC sample is 36.73 ^{o}.

The Braggle angle for Sample 1 is 36.74^{o}, which is not obviously changed. It means that its *d*-spacing was not changed, i.e. its plane did not shift, but the η_{FC} phase transformed into the η_{T} phase proved by the above XRD results. In addition, the Braggle angle for Sample 2 is 36.66^{o}, which is significantly less than that of the raw FC sample and Sample 1, i.e. the Braggle angle for the (0002) plane shifted.

More importantly, in a material removal process, SPD is almost considered constant at the machined surface. Therefore, both of SPD and NPD resulted in phase changes, and only the NPD shifted the preferred crystal orientation but the SPD not. Further, it can be asserted that four-phase transformation took place under high speed cutting after phase decomposition.

4. Conclusions

Ultra-precision raster milling (UPRM) induced external stress results in phase changes at the machined surfaces of Zn-Al alloy, accompanying shear plastic deformation (SPD) and normal plastic deformation (NPD). In this study, their different effects on phase changes of Zn-Al alloy after UPRM with high speed cutting (high strain rate) were firstly discussed, using a series of instruments to detect phase precipitation and phase decomposition, examine preferred crystal orientation, test surface hardness and elastic modulus, and observe chip deformation. Some results have been found as follows:

(1) During UPRM, SPD and NPD both result in phase changes of Zn-Al alloy at its milled surfaces, which is relevant to the cutting and ploughing contributions to chip deformation and surface formation.

(2) Under high strain rate, SPD and NPD induce phase changes of Zn-Al alloy twice, i.e. four-phase transformation takes place after phase decomposition, namely twin phase changes.

(3) Further, it is worth noticing that only NPD causes the shift of preferred crystal orientation of Zn-Al alloy but SPD not.

Acknowledgments

The work was supported by the National Natural Science Foundation of China (Grants no. 51405217 and 51275434), the Youth Science Foundation of Jiangxi Province of China (Grant no. 20142BAB216025) and Jiangxi Educational Committee of China (Grant no. GJJ4210), and the Research Grants Council of the Hong Kong Special Administrative Region (Project no. PolyU 5263/12E).

References

[1] Kao YC, Nguyen NT, Chen MS, Su ST (2015) A prediction method of cutting force coefficients with helix angle of flat-end cutter and its application in a virtual three-axis milling simulation system. Int J Adv Manuf Technol 77:1793-1809

[2] Shaw MC (1984) Metal cutting principles. Clarendon Press, Oxford

[3] Trent EM, Wright PK (2000) Metal cutting. Dutterworth-Heinemann, Boston.

[4] Wyen CF, Wegener K (2010) Influence of cutting edge radius on cutting forces in machining titanium. CIRP Ann Manuf Technol 59:93-96

[5] To S, Zhu YH, Lee WB (2005) Ultra-precision machining induced micro-plastic deformation in Zn-Al based alloy. J Mater Process Technol 167:536-541

[6] Jawahir IS, Brinksmeier E, M'Saoubi R, Aspinwall DK, Outeiro JC, Meyer D (2011) Surface integrity in material removal processes: Recent advances. CIRP Ann Manuf Technol 60:603-626

[7] Wang SJ, Chen X, To S, Ouyang XB, Liu Q, Liu JW, Lee WB (2015) Effect of cutting parameters on heat generation in ultra-precision milling of aluminum alloy 6061. Int J Adv Manuf Technol 80:1265-1275

[8] Fang FZ, Zhang GX (2003) An experimental study of edge radius effect on cutting single crystal silicon. Int J Adv Manuf Technol 22:703-707

[9] Yen YC, Jain A, Altan T (2004) A finite element analysis of orthogonal machining using different tool edge geometries. J Mater Process Technol 146:72-81

[10] Guo YB, Chou YK (2004) The determination of ploughing force and its influence on material properties in metal cutting. J Mater Process Technol 148:368-375

[11] Liu K, Melkote SN (2007) Finite element analysis of the influence of tool edge radius on size effect in orthogonal micro-cutting process. Int J Mech Sci 49:650-660

[12] Wang J, Huang CZ, Song WG (2003) The effect of tool flank wear on the orthogonal cutting process and its practical implications. J Mater Process Technol 142:338-346

[13] Popov Alexey, Dugin Andrey (2014) Effect of uncut chip thickness on the ploughing force in orthogonal cutting: Int J Adv Manuf Technol 76:1937-1945

[14] Popov Alexey, Dugin Andrey (2013) A comparison of experimental estimation methods of the ploughing force in orthogonal cutting. Int J Mach Tools Manuf 65:37-40

[15] Jiang MQ, Dai LH (2009) Formation mechanism of lamellar chips during machining of bulk metallic glass. Acta Mater 57:2730-2738

[16] Liu K, Li XP, Liang SY (2007) The mechanism of ductile chip formation in cutting of brittle materials. Int J Adv Manuf Technol 33:875-884

[17] Zhang SJ, To S, Cheung CF, Zhu YH (2014) Micro-structural changes of Zn-Al alloy influencing micro-topographical surface in micro-cutting. Int J Adv Manuf Technol 72:9-15

[18] Zhu YH, To S, Lee WB, Zhang SJ, Cheung CF (2010) Ultra-precision raster milling-induced phase decomposition and plastic deformation at the surface of a Zn-Al-based alloy. Scr Mater 62:101-104

[19] Chen AY, Ruan HH, Wang J, Chan HL, Wang Q, Li Q, Lu J (2011) The influence of strain rate on the microstructure transition of 304 stainless steel. Acta Mater 59:3697-3709

[20] Choi In-Chul, Kim Yong-Jae, Ahn Byungmin, Kawasaki Megumi, Langdon Terence G, Jang Jae-il (2014) Evolution of plasticity, strain-rate sensitivity and the underlying deformation mechanism in Zn-22% Al during high-pressure torsion. Scr Mater 75:102-105

[21] Wu HB, Zhang SJ (2015) Effects of cutting conditions on the milling process of titanium alloy Ti6Al4V. Int. J. Adv. Manuf. Technol. 77:2235-2240

[22] Zhu YH, Lee WB, To S (2003) Ageing characteristics of cast Zn-Al based alloy (ZnAl7Cu3). J Mater Sci 38:1945-1952